Desalination and Water Treatment
www.deswater.com
doi: 10.1080/19443994.2015.1066713

57 (2016) 14506–14517
July

Taylor & Francis
Taylor & Francis Group

Photocatalyzed ozonation: effective degradation and mineralization of pesticide, chlorothalonil

Suresh Maddila, Surjyakanta Rana, Ramakanth Pagadala, Sreekanth B. Jonnalagadda*

School of Chemistry & Physics, University of KwaZulu-Natal, Westville Campus, Chiltern Hills, Durban 4000, South Africa, Tel. +27 31 260 7325; Fax: +27 31 260 3091; email: jonnalagaddas@ukzn.ac.za (S.B. Jonnalagadda)

Received 5 December 2014; Accepted 19 June 2015

ABSTRACT

The photocatalyzed and ozonated degradation of a widely used pesticide, chlorothalonil was studied using Ru loaded on titania as photocatalyst under visible light. The Ru/TiO_2 photocatalysts with metal loadings 0, 0.25, 0.50, and 1 wt% on TiO_2 were prepared by deposition–precipitation method and characterized by X-ray diffraction, UV-DRS, Brunauer–Emmett–Teller, transmission electron microscopy, SEM–EDX, FT-IR, and ICP analyses. Photocatalyzed ozonation with 1% Ru/TiO_2 yielded 100% degradation and mineralization of chlorothalonil in 2 h under basic pH conditions. The extent of degradation of chlorothalonil pesticide and its mineralization were confirmed by GC–MS. For 10 mg/L of chlorothalonil, 0.1 g/L of catalyst was found to be the optimum for effective mineralization. Results show that photocatalyzed ozonation of chlorothalonil with Ru/TiO_2 catalyst is a very practical means for its mineralization. The catalyst is fully recoverable and reusable multiple times with no loss of activity.

Keywords: Photocatalyst; Ozonation; Chlorothalonil; Ru–TiO_2; Deposition–precipitation method; Mineralization

1. Introduction

Pesticides play prominent role in pest control management and are integral part in modern agriculture. Synthetic pesticides are accepted as a cost-effective means of controlling pests, and refining productivity and food quality [1]. Although pesticides may valuable for agricultural productivity, their persistence in environment has serious implications to the human health, particularly when they are used indiscriminately. As these compounds are chlorine-containing compounds, they are toxic to non-target species and many are non-biodegradable [2–5]. Residues of chemical pesticides in the environment and water systems have become a major issue for both consumers and producers. In view of this, it is prudent to improve technologies that promote the easy degradation of these organic pesticide compounds.

Heterogeneous photocatalysis is an emerging technique for environmental remediation where semiconductor materials are used as photocatalysts [6–9]. Currently, photocatalysis is demonstrated to be as an excellent method over than others due to the use of oxygen as an oxidant, oxidation of the organic compounds at low concentrations, at low temperatures, and comprehensive mineralization [10,11]. Photocatalytic degradation utilizes certain semiconductors as catalysts for the production of the highly reactive

*Corresponding author.

cradicals under light irradiation [12]. The proficiency of this system is based on the production of reactive species, such as hydroxyl radicals, holes, and superoxide anions. However, it is active only under UV irradiation ($\lambda < 387$ nm) because of its wide band gap ($E_g \approx 3.2$), which hinders its further application in the visible light region ($\lambda > 400$ nm) [13–15]. The use of titanium dioxide (TiO_2) as catalyst for the photo-oxidation of aqueous pollutants has significance as it is plentiful, chemically stable, economical, and eco-friendly. The photocatalytic activity of TiO_2 depends on dispersed nature, electron–hole recombination, surface charge, surface morphology, and synthetic approach [15].

A promising technique to execute the mineralization of the substances is the application of advanced oxidation processes by ozone aeration [16–18]. "Catazone" systems, use ozone in the presence of catalyst have been developed in order to enhance the ·OH radical production [19]. Ozone can react with organic matter using two ways: by direct molecular ozone initiated reactions or by indirect pathway leading to ozone decomposition and the generation of ·OH [20]. Attack of ozone on organics leads to the formation of carbonyl compounds and aliphatic acids, which are less reactive to ozone [21,22]. One of the alternatives to gain greater mineralization efficiency is to promote the process via the generation of free hydroxyl radicals, which are more reactive than molecular ozone [23,24]. The decomposition of ozone can take place on different types of active centers. Therefore, basicity and acidity of surface play an important role in the process [24]. In the present study, we report the ozone-facilitated photodecomposition of chlorothalonil, a non-biodegradable pesticide using different loadings of Ru on TiO_2 support as heterogeneous catalyst.

2. Materials and methods

2.1. Preparation of catalysts

The deposition–precipitation method was used in the preparation of metal oxide-supported catalysts [25]. Initially, 1.8 g of TiO_2 (Alfa Aesar Chemical) was suspended in 50 ml of deionized water under vigorous stirring for 45 min. Then, the pH value of this suspension was adjusted with 0.1-M NaOH solution to the desired value, using a computer-based pump system linked to a pH meter. The suspension was kept at pH under stirring for additional 2 h. In parallel, 20 mL of deionized water and 1.5 mL of 0.1 M NaOH solution are mixed in another beaker. Then, 1.8 mL of 0.2-M ruthenium(III) chloride hydrate aqueous solution (Aldrich, 99.98% trace metals basis) was added, and the mixture was stirred once. This solution was preserved for 1.5 h. After, the ruthenium aqueous solution was added into the TiO_2 suspension under stirring. For the period of addition of the ruthenium solution, the pH was maintained at the same value as before the addition via adjustment with 0.1-M NaOH solution using a pH meter. The suspension was vigorously stirred for another 2 h. All of the steps described pH value of 10 were maintained. The precipitate was aged at 60–70˚C for 1 h in the mother solution and filtered and washed with deionized water for three times. The samples were dried at 130–140˚C for overnight and then calcined in the presence of air, at 450˚C for 4 h to obtain the 0.25, 0.50, and 1% w/w of Ru/TiO_2 catalysts.

2.2. Instrumentation

2.2.1. Characterization of catalysts

The different metal oxide phases in the catalysts were observed using powder X-ray diffraction (XRD) performed on a Bruker D8 Advance instrument, equipped with an Anton Paar XRK 900 reaction chamber, a TCU 750 temperature control unit, and a Cu Kα radiation source with a wavelength of 1.5406 nm at 40 kV and 40 mA. Diffractograms were recorded over the range of 15˚–90˚ with a step size of 0.5 per second. The Brunauer–Emmett–Teller (BET) surface area, total pore volume, and average pore size were measured using a Micrometrics Tristar II surface area and porosity analyzer. Prior to the analysis, the powdered samples (~0.180 g) were degassed under N_2 for 12 h at 200˚C using a Micrometrics Flow Prep 060 instrument. Textural properties of catalyst samples were measured by N_2 adsorption–desorption isotherms obtained at −196˚C. The SEM measurements were carried out using a JEOL JSM-6100 microscope equipped with an energy-dispersive X-ray analyzer (EDX). The images were taken with an emission current = 100 μA by a Tungsten (W) filament and an accelerator voltage = 12 kV. The catalysts were secured onto brass stubs with carbon conductive tape, sputter coated with gold, and viewed in JEOL JSM-6100 microscope. The transmission electron microscopy (TEM) images were viewed on a Jeol JEM-1010 electron microscope. The images were captured and analyzed using iTEM software. The particle sizes obtained were the average particle size of 40–60 particles and the standard deviation is done in order to determine the range of the particle sizes. High-resolution TEM images were recorded using Jeol JEM 2100 Electron Microscope. Infrared spectra of the samples were recorded using Fourier transmission infrared (FTIR) spectrometer

(PerkinElmer spectrum 100 series with universal ATR accessory). UV–vis diffuse reflectance spectra were recorded with an Ocean Optics high-resolution spectrometer (HR2000+) equipped with an integrating sphere accessory, using $BaSO_4$ as a reference. Inductively coupled plasma optical emission spectrometer (ICP-OES) (Optima 5300 DV) was used in analyzing the concentration of the elements present in the samples after digesting in concentrated H_2SO_4.

2.2.2. Characterization of the products

The GC–MS analysis was carried out in EI mode and the spectra were recorded in the interval 35–500 amu. For analysis of compounds, Agilent 6890 gas chromatograph equipped with a quadruple Agilent 5973n mass selective detector was used. Column specifications: J & W DB5MS, 30-m length, 250-μm diameter and 0.25-μm film thickness. The temperature program used during the GC–MS analysis was ramped as follows: 50˚C (2 min), 20˚C min^{-1} until 300˚C (10 min). The sample was carried out with a 1.50 min split-less time at 250˚C. The carrier used was helium. The mass spectra were recorded on an Agilent 1100 LC/MSD instrument, with method API-ES, at 70 eV. ^1H NMR (400 MHz) spectra were recorded on a Bruker AMX 400 MHz NMR spectrometer in $CDCl_3$/DMSO-d_6 solution using TMS as an internal standard. All chemical shifts are reported in δ (ppm) using TMS as an internal standard. The mass spectra were recorded on an Agilent 1100 LC/MSD instrument, with method API-ES, at 70 eV.

2.2.3. Photocatalytic ozonation experiment

The chlorothalonil degradation experiments were carried out in a simple photocatalyzed ozonation reactor using visible light (Fig. 1). The cylindrical photoreactor of capacity 500 mL which is provided with a water jacket for maintaining the temperature at (20 ± 1)˚C and a magnetic stirrer to keep the reaction mixture in suspension. The light was provided by a high-pressure mercury lamps (8 W; 365 nm) or halogen lamp with filter (125 W) for visible irradiations, respectively. It was arranged in the center of the reactor and cooled by a water jacket. Ozone was generated using a Fischer Ozone 500 generator, which produced ozone by the electric discharge of oxygen from a compressed oxygen cylinder via the corona discharge method. Chlorothalonil solution was prepared by dissolving in double-distilled water. The temperature was kept at 20 ± 1˚C during all the experiments. For *Visible light* (*Vis*) + O_3 experiment, the specific concentration of chlorothalonil (10 mg/L) was preserved in the reactor and ozone was passed in to the solution with continuous stirring. The amount of ozone was estimated by volumetric method trapping it in KI solution and titrating the liberated iodine using standard thiosulfate solution with starch as indicator [26,27]. Flow rates and ozone concentrations were calibrated and highly reproducible. Parameters were checked in duplicate runs, prior to and after each of the experiments. The same procedure was adopted in without light. For catalyst/visible experiments, before the light irradiation, 0.1 g of the photocatalyst was added to 250 mL of chlorothalonil (10 mg/L) aqueous solution, and then the mixture was thoroughly mixed using an ultrasound bath for 20 min, to disperse the powder. The mixture was then kept in the dark for 1 h, with continual stirring using a magnetic stirrer bar, to reach the adsorption–desorption equilibrium. Samples were collected at specified intervals of time and centrifuged at 3,500 rpm, filtered, and taken for analysis. The same procedure was repeated for catalyst/UV/O_3 experiments.

3. Results and discussion

3.1. Catalyst testing and product identification

All the photocatalyzed ozone aeration semi-batch experiments were conducted by exposing the reaction mixtures with visible light and with a continuous flow of ozone-enriched oxygen stream. After a specified period of ozone aeration, the organic portion of the reaction mixture was extracted and analyzed after every reaction with 20 min intervals. The three products identified by GC–MS (Fig. 2). The peaks from 9.00 to 13.60 retention times refer to the intermediates and various aliphatic carboxylic acid compounds formed due to the further oxidation of the products of the reaction. Based on the mass spectra and the reference standards, the first oxidation product was confirmed to be 2,4-dinitrile-3-hydroxy-4-oxo-2-butenoic acid (DNHBA), the second product was 2-cyano-2-oxoacetic acid (CAA) and the third product was Oxalic acid (OA). The ^1P NMR spectrum of DNHBA showed a broad singlet for the COOH group at δ 11.96 ppm and singlet at δ 9.12 ppm for the OH group, respectively. The mass spectrum showed m/z peak at 165 (M–H). Similarly compound CAA displayed a broad singlet at δ 11.35 ppm for COOH proton. Moreover, the mass spectrum showed at m/z at 99 (M^+). Finally, compound OA displayed a broad singlet peak for COOH groups at δ 13.08 ppm. The mass spectrum showed m/z peak at 91 (M + H). These are the good agreement with spectra of the ^1H NMR and mass values in the

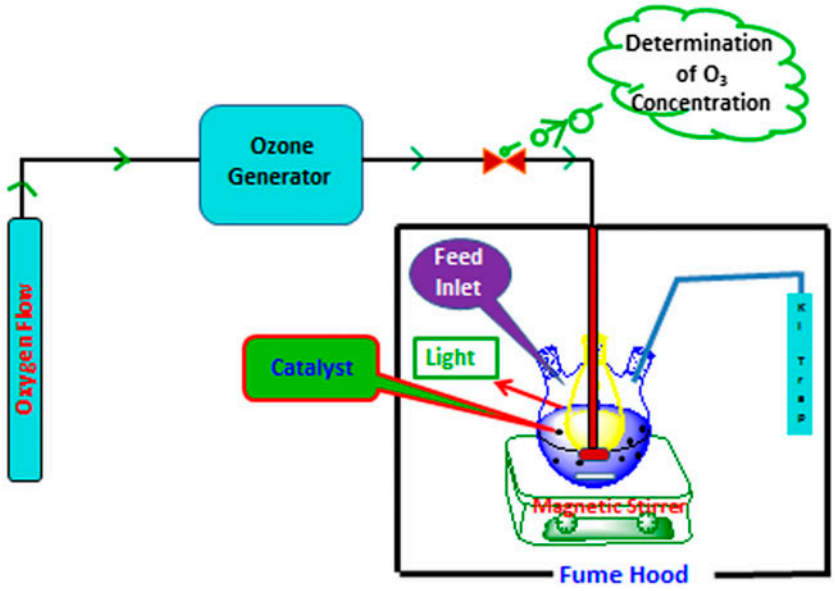

Fig. 1. Experimental set up for photocatalytic ozonator.

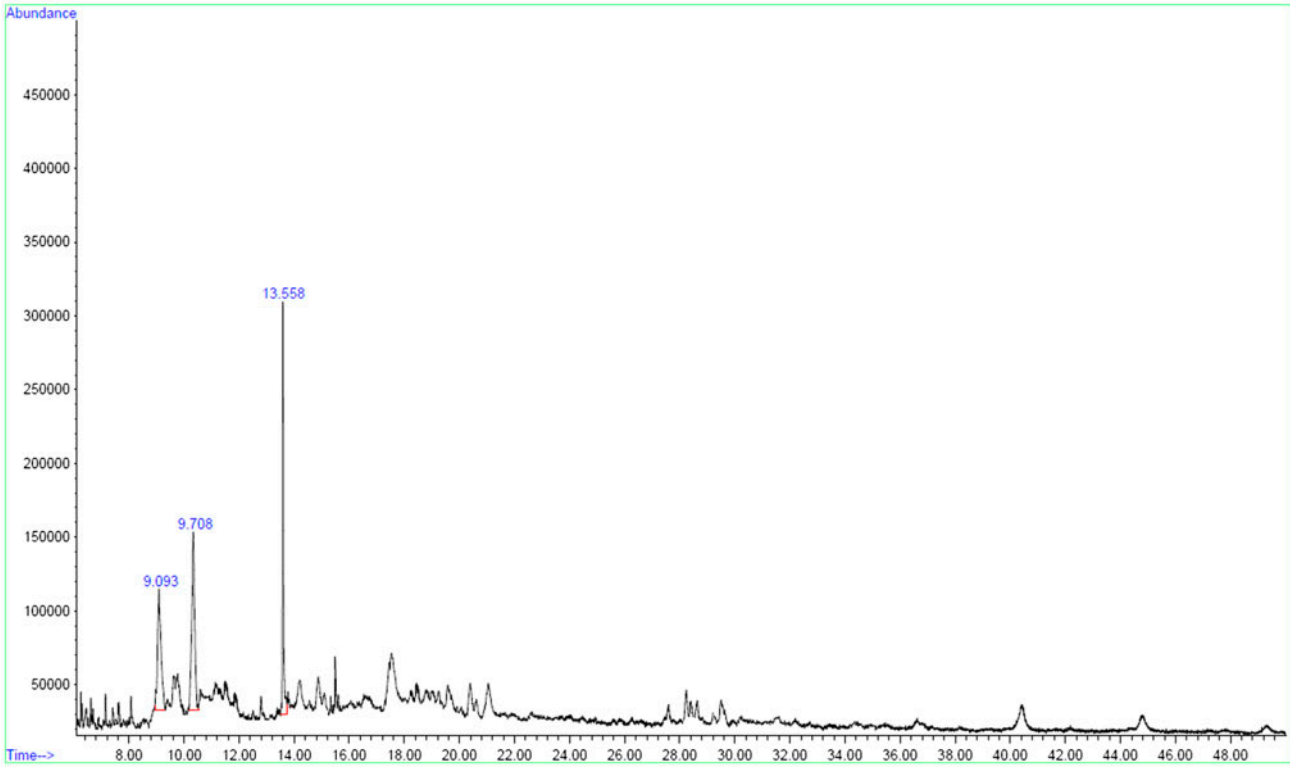

Fig. 2. GC–MS chromatogram of product mixture.

products. Further, the qualitative test (lime water) confirmed the release of CO_2 during the reactions and suggested some mineralization of pesticides. Photocatalytic ozonation of pesticides in water is known to produce more biodegradable oxygenated organic products and low-molecular weight acids.

3.2. BET surface area and elemental analysis (BET and ICP)

The N_2 adsorption–desorption study was carried out over (a) bare TiO_2, (b) 0.25% Ru–TiO_2, (c) 0.5% Ru-TiO_2, and (d) 1% Ru–TiO_2 (Fig. 3). N_2 adsorption–desorption resulted in typical type-II isotherm, with a H1 hysterisis loop, for both the materials as defined by Sing et al. The initial increase in N_2 uptake at low p/p_o may be due to monolayer adsorption on the pore walls, a sharp steep increase at intermediate p/p_o indicates the capillary condensation in the mesopores, and a plateau portion at higher p/p_o is associated with multilayer adsorption on the external surface of the materials [28].

Bare TiO_2 exhibits N_2 uptake at a relative pressure of 0.3 which corresponds to the pre-condensation loop. The isotherm shows a H1-type hysteresis loop with well-developed step in the relative pressure range ≈0.9. The incorporation of Ru in the TiO_2 framework is found to higher the p/p_o value for capillary condensation step, indicating the shift in pore size to higher value. The pore diameter is found to increase with increase in loading of Ru content over the TiO_2 surface.

The textural properties such as BET surface area, pore diameter, and pore volume derived from the N_2 adsorption–desorption measurements are included in Table 1. The parent TiO_2 has a surface area of 79.14 m^2/g but a gradual increase in the value with increase in Ru content in TiO_2 was observed. This may be due to the increase in the active phages of Ru onto support surface. Pore size and pore volume exhibit similar trend as that of surface area with a gradual increase in the values with increasing Ru % on TiO_2. The ICP-OES analysis confirmed the presence of respective amounts of Ru in the catalyst materials.

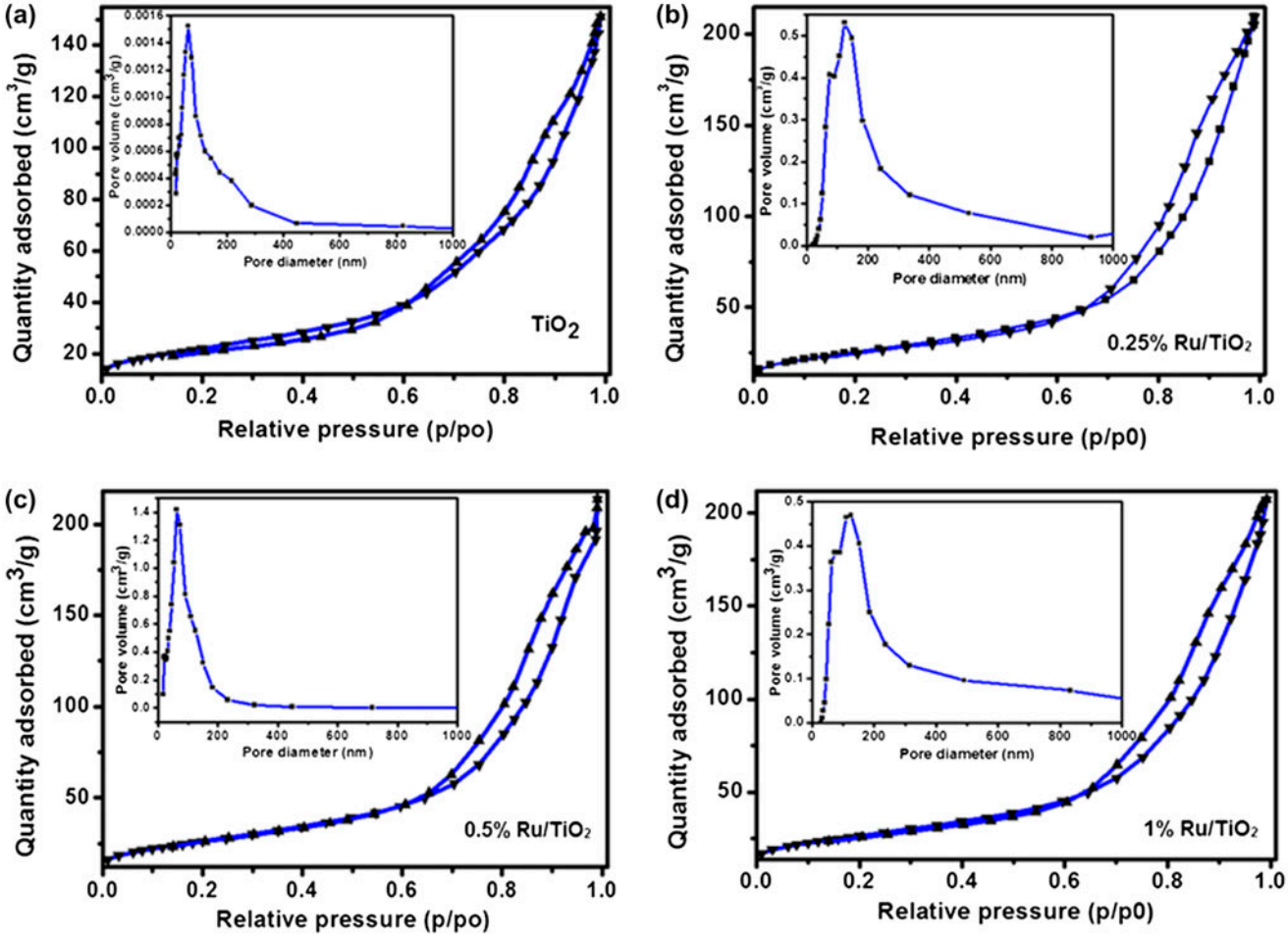

Fig. 3. N_2-adsorption & desorption spectra and pore size distribution curve of (a) bare TiO_2, (b) 0.25% Ru/TiO_2, (c) 0.5% Ru/TiO_2, and (d) 1% Ru/TiO_2.

Table 1
BET surface area, elemental analysis and bandgap of Ru loaded supports

Catalyst	Ru wt% (from ICP)	Surface area (m^2/g)	Pore size (nm)	Pore volume (cm^3/g)	Ru wt% (from EDX)	Band gap (eV)
Bare TiO_2	–	79.14	10.4	0.2068	–	3.20
0.25Ru–TiO_2	0.24	92.22	11.9	0.2903	0.24	2.87
0.5Ru–TiO_2	0.49	94.72	12.5	0.2966	0.48	2.79
1Ru–TiO_2	0.98	96.27	12.9	0.2997	0.99	2.69

3.3. Fourier transform infrared spectroscopy (FT-IR)

The FT-IR spectrum of bare TiO_2 and Ru doped TiO_2 catalysts is shown in (Fig. 4). The sequences of bands seeming in these spectra are corresponding to the various lattice vibrational modes. The broad peaks in the range of 3,000–3,400 cm^{-1} attributed from surface adsorbed water and surface hydroxyl group, respectively [29]. The sharp peaks observed at 1,630 cm^{-1} for all the catalysts may be originated to the bending vibrations of adsorbed water molecules whereas the peaks observed around 650 cm^{-1} are due to the vibrational modes of Ti–O–Ti. After modification of Ru over titania surface, adsorption peaks are shifted to the lower wave number.

3.4. X-ray diffraction (XRD)

The crystallinity of the prepared samples was examined by XRD analysis. The PXRD pattern of (a) bare TiO_2, (b) 0.25% Ru–TiO_2, (c) 0.5% Ru–TiO_2, (d) 1% Ru–TiO_2 is shown in the Fig. 5. This pattern gives the information of phases and structure of the prepared samples. The peak values at 25.3, 30.8, 37.8, 48.1, 53.9, 54.3, 56.6, 70.2, 75.1, and 82.7 were identified by comparison with literature data and confirm that the particles are crystalline with an anatase structure [30]. The PXRD patterns of different wt% Ru loaded TiO_2 corresponds to anatase phase (JCPDS 06-0663 & JCPDS 83-2243). A reflection due to ruthenium is observed at 27.4° and 36.1°. From this, it is clear that the content of RuO_2 has an influence on the particle size of anatase, which decreases with increase in amounts of RuO_2. The crystallization degree of the anatase could be confirmed from the XRD patterns.

3.5. Scanning electron microscopy–EDX (SEM–EDX)

To study the surface morphology and to assess the dispersion of the active components over the surface of TiO_2, SEM investigation was performed for (a) Bare TiO_2, (b) 0.25% Ru/TiO_2, (c) 0.5% Ru/TiO_2, and (d) 1% Ru/TiO_2 are shown in the Fig. 6. From the SEM images, it is conform that TiO_2 is spherical particles of particle size around 30–40 nm. After different wt% of Ru modified on the titania support, the morphology of catalyst changes i.e. it comes to rod-like shape. The rod -like morphology depends upon the amount of ruthenium incorporates on support surface [31]. From lower to higher wt%, all the crystals showed good growth. EDAX investigation was performed to get information about the presence of the surface composition of the active components like (a) bare TiO_2,

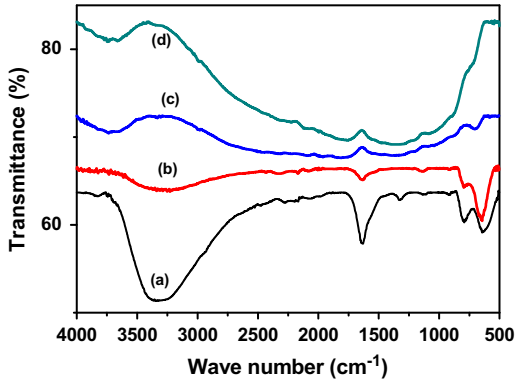

Fig. 4. FT-IR spectra of (a) bare TiO_2, (b) 0.25% Ru/TiO_2, (c) 0.5% Ru/TiO_2, and (d) 1% Ru/TiO_2.

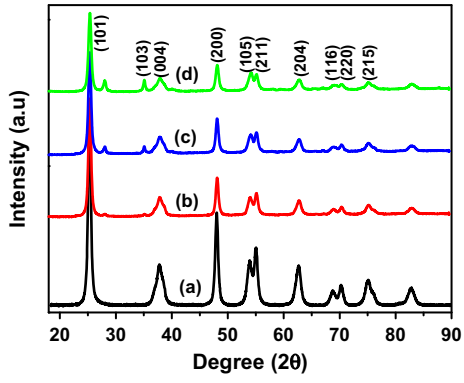

Fig. 5. XRD spectra of (a) bare TiO_2, (b) 0.25% Ru/TiO_2, (c) 0.5% Ru/TiO_2, and (d) 1% Ru/TiO_2.

(b) 0.25% Ru/TiO_2, (c) 0.5% Ru/TiO_2, and (d) 1% Ru/TiO_2 are shown in the Fig. 6. EDX analysis showed successful dispersion of ruthenium on the surface of TiO_2 sample. It showed that ruthenium was homogenously dispersed on the surface of TiO_2 and the EDX analysis results are in agreement with the ICP analysis results.

3.6. Transmission electron microscopy (TEM)

Fig. 7 shows the typical TEM images of the ruthenium-supported TiO_2 catalysts. The TEM images clearly illustrated twin boundaries due to the presence of ruthenium on TiO_2 surface [32]. From this image, the bare titania is amorphous shape. After ruthenium modification on the titania surface, the morphology changes like rod-like shape. From lower wt% to higher wt% of Ru is on the titania surface, the crystals are well grown. It is one-dimensional nanorod. Selected areas of the SAED electron diffraction patterns confirm the presence of anatase and RuO_2 phases Fig. 7(e).

3.7. UV–vis DRS and photoluminescence spectra

The bandgap measurements from diffuse reflectance studies will cover way to understand the optical response of the catalysts. From the DRS spectra, the bandgap values for all the catalysts were designed using the formula E (eV) = 1,240/λ and specified in Table 1. While pure titania exhibited the maximum bandgap value of 3.20 eV, Ru-loaded materials exhibited lower bandgap. Reddy et al. too observed a slight decrease in the band-gap values for ruthenium impregnated titania catalysts [33]. The shifting of optical response of doped catalysts to visible area can well be understood from the decrease in the band-gap value from 3.2 eV. The intensity of the absorbance in the visible region increases with the concentration of the doped ruthenium ion. Catalysts showing such red shift are generally photocatalytically active in the visible region. The drop in TiO_2 band gap is due to the presence of the dopant. A shift in the band gap of TiO_2 may be attributed to its crystallinity [34], and hence the possibility for new energy levels.

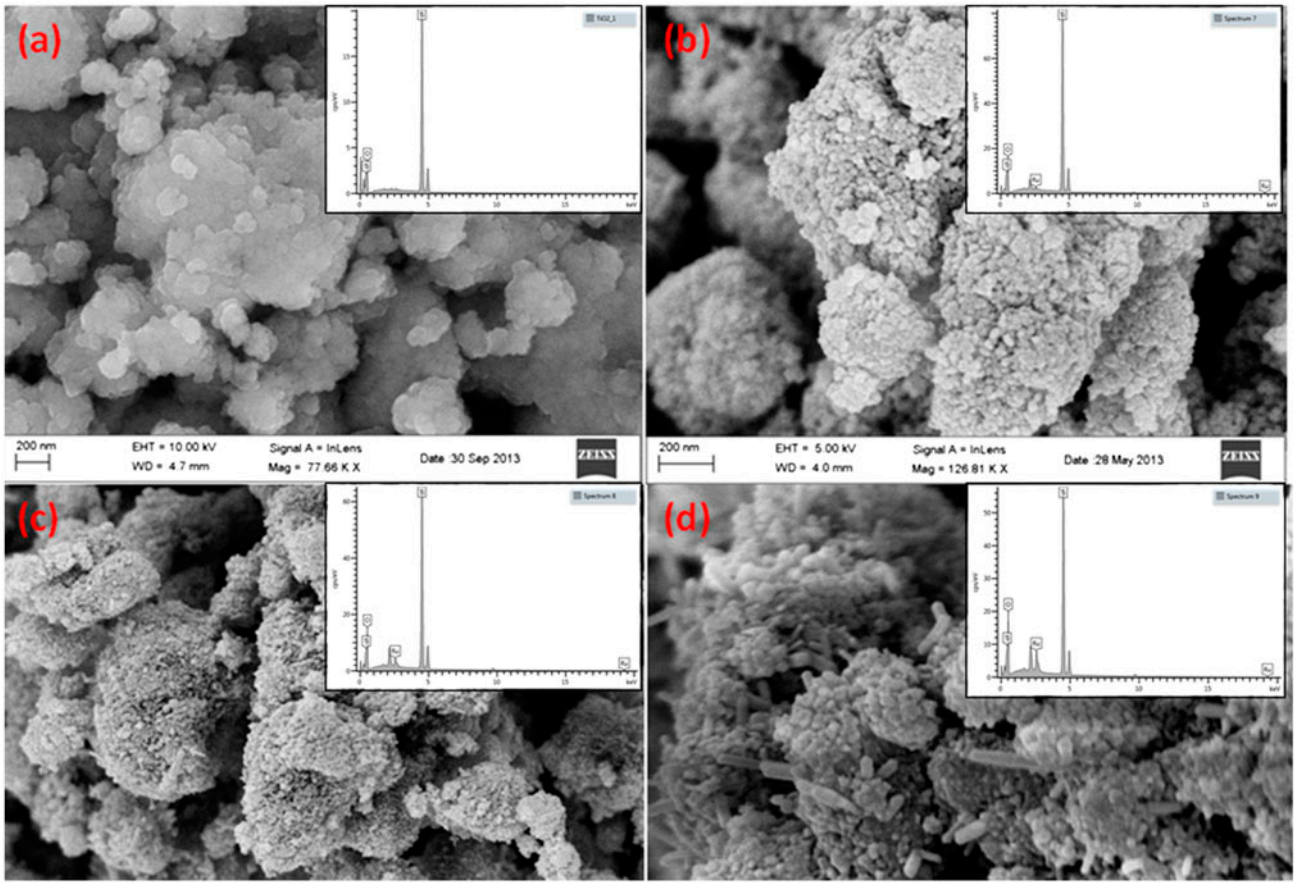

Fig. 6. SEM and SEM–EDX spectra of (a) bare TiO_2, (b) 0.25% Ru/TiO_2, (c) 0.5% Ru/TiO_2, and (d) 1% Ru/TiO_2.

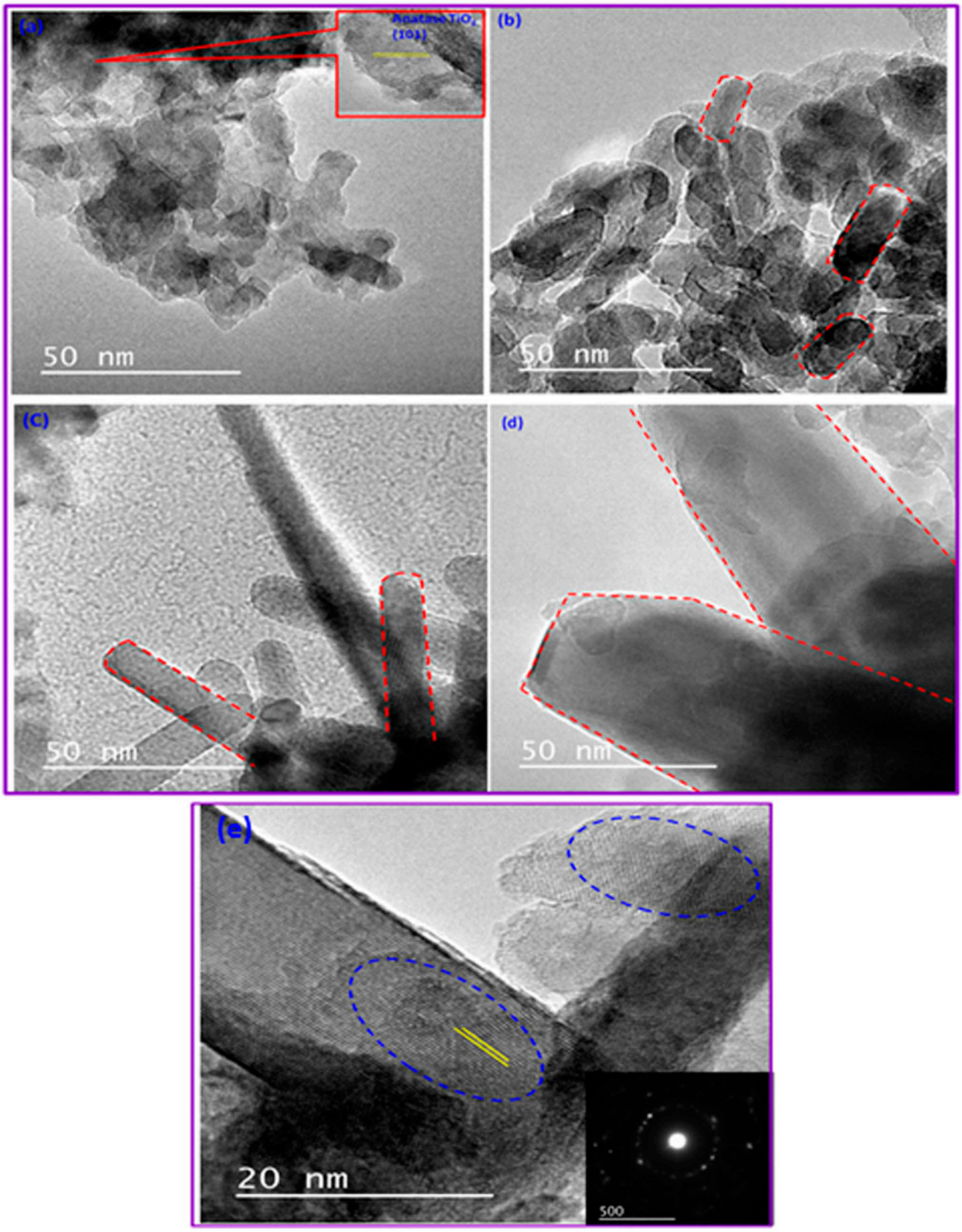

Fig. 7. TEM image of (a) bare TiO_2, (b) 0.25% Ru/TiO_2, (c) 0.5% Ru/TiO_2, (d) 1% Ru/TiO_2, and (e) 1% Ru/TiO_2 (inset in SAED image).

Photoluminescence (PL) emission spectra have been used to study the transfer behavior of the photogenerated electrons and holes for the understanding the separation and recombination of photogenerated charge carriers [35]. The PL intensity greatly decreased after the loading of Ru. Ru deposits could act as trapping sites to capture photogenerated electrons from titania conduction band, separating the photogenerated electron–hole pairs [36]. Therefore, the recombination rate of photogenerated electrons and holes was retarded, leading to the reduction of PL signal decrease. And it was also found that 1.0% Ru/TiO_2 showed lower PL intensity, which may be attributed to its higher Ru content. It was reported in the literature [37] that the ruthenium oxide coupled with titania could form the composite semiconductor and the electrons which were generated by UV-light illumination could move from TiO_2 into RuO_2 particles due to their conduction band offset. Thus, the lifetime of hole–electron pairs generated was prolonged.

3.8. Role of Ru doping concentrations

Photo-oxidation of chlorothalonil in the presence of pure TiO_2 and Ru loaded on TiO_2 was carried out in order to study the photocatalytic oxidation activity under visible light. The photocatalytic oxidation activity of photocatalyst was significantly enhanced on the addition of ruthenium. The removal efficiency increased from these catalysts. Further, the photocatalytic oxidation activity of Ru-doped TiO_2 increased with the increase in doping concentration of ruthenium (up to 1.0%). An increase in the amount of Ru dopant resulted in the increase in visible light absorption and hence enhanced photocatalytic oxidation activity. The optimal degradation of chlorothalonil was found to be at 1.0 wt% Ru concentration with the removal efficiency of 100%.

3.9. Role of 1% Ru/TiO_2 loading

The photocatalytic ozone degradation of chlorothalonil was carried out over a 1.0% Ru/TiO_2 catalyst at a different loading of 5–15 mg/L in order to optimize catalyst loading during the visible irradiation process. A significant increase in the degradation of chlorothalonil as catalyst loading increases from 5 to 15 mg/L. The decrease in the degradation of chlorothalonil above 10 mg/L may be attributed to the scattering effect of light caused by the high concentration of photocatalyst. The photodecomposition rates of pollutants are influenced by the active site and the photoabsorption of the catalyst used. Adequate loading of the catalyst increases the generation rate of electron/hole pairs for enhancing the degradation of pollutants. However, addition of a high dose of the semiconductor decreases light penetration by the photocatalyst suspension and reduces degradation rate [37].

3.10. Effect of pH

The pH of solution may influence the surface properties of catalyst, charge of the pollutants, and

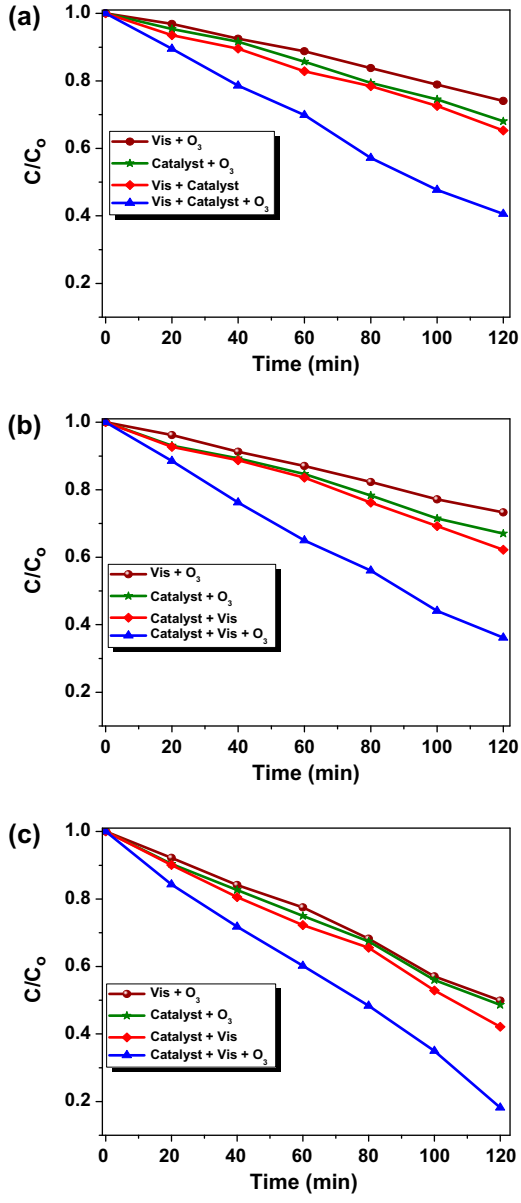

Fig. 8. Time course of the ratio of C/C_o for different photo-oxidations at (a) pH 3, (b) pH 7, and (c) pH 11 concentration of chlorothalonil = 10 mg/L, mass of 1% Ru/TiO_2 = 0.1 g/L, temperature = 20 ± 1°C.

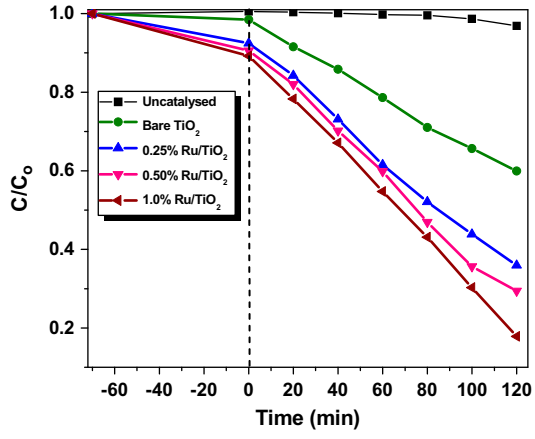

Fig. 9. Photocatalytic activities of the 1% Ru/TiO_2 catalysts in degrading chlorothalonil (pH 11).

generation of free radicals [38]. Therefore, the study of pH influence on the photocatalytic ozonation process would be helpful to understand the mechanism of the process as well as for a higher degree of removal. The influence of pH on the effectiveness of chlorothalonil degradation by ozonation is shown in Fig. 8. The degradation experiments were carried out at pH values of 3, 7, and 11. The degradation rate increased as the pH increased from 3 to 11. Under acidic pH, O_3 molecule is main reactive species and its reactivity is very low relative to hydroxyl radical, so the degradation of chlorothalonil is very low. As the solution becomes more basic, the rate of photocatalyzed decomposition of ozone to secondary oxidants, such as hydroxyl radicals increases. While the increase in pH facilitates the hydroxyl radical concentration, the effect of pH on the substrate reactivity is also equally vital for efficient conversion. The obtained results indicate that the process effectiveness increases significantly and highest conversion was recorded at pH 11.

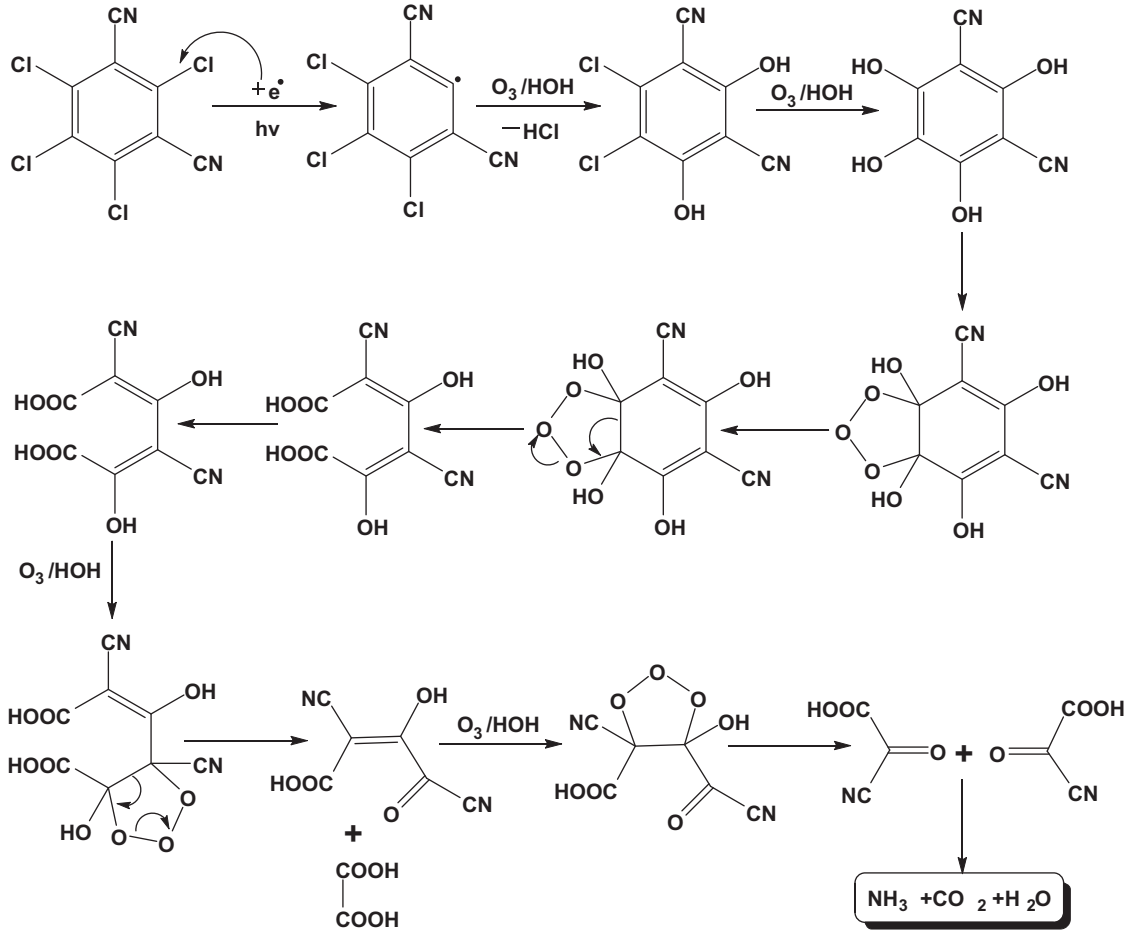

Fig. 10. Proposed reaction mechanism.

3.11. Photocatalytic activity Ru/TiO_2

The photocatalyzed ozone facilitated degradation of chlorothalonil in presence of pure TiO_2 and various wt% of Ru on TiO_2 is illustrated in Fig. 9. A perusal of figure clearly shows that the photodegradation of Ru-doped titania catalysts is far efficient than that of pure TiO_2, which confirms that Ru doping enhances the photocatalytic activity of pure TiO_2. The probable reasons are: (a) Ru ion doping makes the doped samples have smaller average crystal size and absorb more visible light to generate more electron–hole pairs and/or (b) Ru can interact directly with the organic molecules, and the electrons surrounded by ruthenium are efficiently transferred to the adsorbed O_2 to generate superoxide anion radicals, which is beneficial to react with the organics.

Fig. 9 also show that the photocatalytic activity of $Ru–TiO_2$ enhanced by wt% of Ru doped on the support. The sample of $Ru–TiO_2$ with 1% Ru ion doping shows the highest photocatalytic activity. Ruthenium can capture electrons to accomplish a higher photocatalytic activity with an appropriate doping concentration. Excessive Ru doping concentration is expensive and may also result in the recombination of photogenerated electron–hole pairs resulting in decrease in the photcatalytic activity. Hence, higher loading of Ru > 1 wt% was not tested.

The phenomenon of photocatalyzed degradation of chlorothalonil in presence of ozone probably occurs through the cleavage of the chlorothalonil pesticide chloro groups from aromatic compound (Fig. 10). In substituted aromatics, chloro and cyano are very good leaving groups; the ozone or hydroxyl radical attack leads to dechlorination and formation of phenoxy radical. Phenoxy radicals get transformed to phenol, through further attack by ·OH. The transient intermediate, 2,4-dihydroxy-3,5-dinitrile-1,6-dicarboxylic acid favoring the electrophilic substitution of ·OH at the cyano position forms a stable intermediate, 2-cyano-2-oxoacetic acid (via oxidation). The further oxidation of cyano-2-oxoacetic acid by ·OH leads to oxygenated aliphatic compounds and formation of degraded to aliphatic carboxylic acids. Oxalic acid was identified in this study. Further oxidation of the reaction products leads to complete mineralization to CO_2 and H_2O.

4. Conclusions

A combination of photocatalysis and ozonation proved to be effective in dechlorination and mineralization of chlorothalonil. The $Ru–TiO_2$ catalysts were successfully prepared by deposition–precipitation method and characterized. Ru doping possibly decreases the recombination of photogenerated electron–hole pairs, acting as the capture of photo-holes. Compared with pure TiO_2, the light absorption edge of $Ru–TiO_2$ is redshift. After 2 h reaction, about 65% of substrate got oxidized at neutral pH, while at pH 11, the extent of oxidation was 85%. The results conclude that 1% Ru/TiO_2 could be an ideal catalyst for the photocatalyzed ozonated degradation of chlorothalonil. The catalyst activity is found to be sustainable and catalyst is recyclable with no significant loss of activity.

Acknowledgments

The authors are indebted to the National Research Foundation, South Africa, for financial support and University of KwaZulu-Natal, Durban, South Africa for the research facilities.

References

[1] K. Virender, S. Uma, M.K. Khushu, Bio-intensive integrated pest management in fruit crop ecosystem, Integr. Pest Manage.: Innovat. Develop. Proc. 1 (2009) 631–666.
[2] Md.W. Aktar, D. Sengupta, A. Chowdhury, Impact of pesticides use in agriculture: Their benefits and hazards, Interdisc. Toxicol. 2 (2009) 1–12.
[3] S. Maddila, L. Palakondu, S.B. Jonnalagadda, Degradation, mineralization of bromoxynil pesticide by heterogeneous photocatalytic ozonation, J. Ind. Eng. Chem. 24 (2015) 334–341, doi: 10.1016/j.jiec.2014.10.005.
[4] S. Chiron, A. Fernandez-Alba, A. Rodriguez, E. Garcia-Calvo, Pesticide chemical oxidation: State-of-the-art, Water Res. 34 (2000) 366–377.
[5] S.A. Greene, R.P. Pohanish, Sittig's Handbook of Pesticides and Agricultural Chemicals, William Andrew Publishing, New York, 2005.
[6] M. Pelaez, N.T. Nolan, S.C. Pillai, M.K. Seery, P. Falaras, A.G. Kontos, P.S.M. Dunlop, J.W.J. Hamilton, J.A. Byrne, K. OShea, Md.H. Entezarig, D.D. Dionysiou, A review on the visible light active titanium dioxide photocatalysts for environmental applications, Appl. Catal. B: Environ. 125 (2012) 331–349.
[7] M. Arias-Estevez, E. Lopez-Periago, E. Martínez-Carballo, J. Simal-Gandar, M. Juan-Carlos, L. Garcia-Rio, The mobility and degradation of pesticides in soils and the pollution of groundwater resources, Agric. Ecosyst. Environ. 123 (2008) 247–260.
[8] G.C. López-Pérez, M. Arias-Estévez, E. López-Periago, B. Soto-González, B. Cancho-Grande, J. Simal-gaa Ndara, Dynamics of pesticides in potato crops, J. Agric. Food Chem. 54 (2006) 1797–1803.
[9] Y. Zhang, J.W.C. Wong, P. Liu, M. Yuan, Heterogeneous photocatalytic degradation of phenanthrene in surfactant solution containing TiO_2 particles, J. Hazard. Mater. 191 (2011) 136–143.

[10] K. Kavita, C. Rubina, L.S. Rameshwar, Treatment of hazardous organic and inorganic compounds through aqueous-phase photocatalysis: A Review, Ind. Eng. Chem. Res. 43 (2004) 7683–7696.
[11] N.C. Meng, J. Bo, W.K. Christophex, C.S. Chow, Recent developments in photocatalytic water treatment technology: A review, Water Res. 44 (2010) 2997–3027.
[12] O. Tsuyoshi, F. Akira, Photoelectrochemical properties of TiO_2 photocatalyst and its applications for environmental purification, J. Photochem. Photobiol. C: Photochem. Rev. 13 (2012) 247–262.
[13] C. Chen, W. Ma, J. Zhao, Semiconductor-mediated photodegradation of pollutants under visible-light irradiation, Chem. Soc. Rev. 39 (2010) 4206–4219.
[14] S. Maddila, E.O. Oseghe, S.B. Jonnalagadda, Photocatalysed ozonation by Ce doped TiO_2 catalyst degradation of pesticide, Dicamba in water, J. Chem. Technol. Biotechnol. (in press), doi: 10.1002/jctb.4583.
[15] X.Z. Li, F.B. Li, Study of Au/Au^{3+}–TiO_2 photocatalysts toward visible photooxidation for water and wastewater treatment, Environ. Sci. Technol. 35 (2001) 2381–2387.
[16] T.E. Agustina, H.M. Ang, K. Vareek, A review of synergistic effect of photocatalysis and ozonation on wastewater treatment, J. Photochem. Photobiol. C: Photochem. Rev. 6 (2005) 264–273.
[17] E.C. Chetty, V.B. Dasireddy, S. Maddila, S.B. Jonnalagadda, Efficient conversion of 1,2-dichlorobenzene to mucochloric acid with ozonation catalyzed by V_2O_5 loaded metal oxides, Appl. Catal. B: Environ. 117–118 (2012) 18–28.
[18] E.C. Chetty, S. Maddila, C. Southway, S.B. Jonnalagadda, Ozone initiated Ni/metal oxide catalyzed CONVERSION of 1,2-dichlorobenzene to mucochloric acid in aqueous solutions, Ind. Eng. Chem. Res. 51 (2012) 2864–2873.
[19] V.S.S.R. Rajasekhar Pullabhotla, S.B. Jonnalagadda, Scope of metal loaded microporous ZSM-5 zeolites in the "catazone" process of *n*-hexadecane at moderate conditions, Ind. Eng. Chem. Res. 48 (2009) 9097–9105.
[20] M.J. Farré, M.I. Franch, S. Malato, J.A. Ayllón, J. Peral, X. Doménech, Degradation of some biorecalcitrant pesticides by homogeneous and heterogeneous photocatalytic ozonation, Chemosphere 58 (2005) 1127–1133.
[21] S. Maddila, V.D.B.C. Dasireddy, S.B. Jonnalagadda, Ce–V loaded metal oxides as catalysts for dechlorination of chloronitrophenol by ozone, Appl. Catal. B: Environ. 150–151 (2014) 305–314.
[22] S. Maddila, V.D.B.C. Dasireddy, E.O. Oseghe, S.B. Jonnalagadda, Ozone initiated dechlorination and degradation of trichlorophenol using Ce–Zr loaded metal oxides as catalysts, Appl. Catal. B: Environ. 142–143 (2013) 129–141.
[23] M.M. Huber, S. Canonica, G.-Y. Park, U. von Gunten, Oxidation of pharmaceuticals during ozonation and advanced oxidation processes, Environ. Sci. Technol. 37 (2003) 1016–1024.
[24] S.B. Jonnalagadda, V.S.S.R. Pullabhotla, S. Maddila, E.C. Chetty, Ozone for drinking and wastewater treatment and for value added products, Int. J. Chem. 1(1) (2012) 119–129.
[25] A. Corma, H. Garcia, Supported gold nanoparticles as catalysts for organic reactions, Chem. Soc. Rev. 37 (2008) 2096–2126.
[26] Standard Methods for the Examination of Water and Wastewater, American Public Health Association/American Water Works Association/Water Environment Federation, 20th ed., Washington, DC, 1998.
[27] S. Maddila, V.D.B.C. Dasireddy, S.B. Jonnalagadda, Dechlorination of tetrachloro-o-benzoquinone by ozonation catalyzed by cesium loaded metal oxides, Appl. Catal. B: Environ. 138–139 (2013) 149–160.
[28] K.S.W. Sing, D.H. Everett, R.A. Haul, W.L. Moscou, R.A. Pierotti, J. Rouquérol, T. Siemieniewska, Reporting physisorption data for gas/solid systems with special reference to the determination of surface area and porosity, Pure Appl. Chem. 57 (1985) 603–619.
[29] G. Liu, X. Wang, Z. Chen, H.-M. Cheng, G. Lu, The role of crystal phase in determining photocatalytic activity of nitrogen doped TiO_2, J. Colloid Interface Sci. 329 (2009) 331–338.
[30] P. Kluson, L. Cerveny, J. Had, Preparation and properties of ruthenium supported catalysts, Catal. Lett. 23 (1994) 299–312.
[31] O. Mitsumasa, S. Osamu, A. Kunio, S. Masayuki, Stability of supported ruthenium catalysts for lignin gasification in supercritical water, Energy Fuels 20 (2006) 2337–2343.
[32] X. Shen, L.J. Garces, Y. Ding, K. Laubernds, R.P. Zerger, M. Aindow, E.J. Neth, S.L. Suib, Behavior of H_2 chemisorption on Ru/TiO_2 surface and its application in evaluation of Ru particle sizes compared with TEM and XRD analyses, Appl. Catal. A: Gen. 335 (2008) 187–195.
[33] K.M. Reddy, S.V. Panorama, A.R. Reddy, Bandgap studies on anatase titanium dioxide nanoparticles, Mater. Chem. Phys. 78 (2002) 239–245.
[34] H. Vendula, S. Vaclav, B. Snejana, M. Nataliya, T. Vaclav, Efficient gas phase photodecomposition of acetone by Ru-doped titania, Appl. Catal. B: Environ. 89 (2009) 613–619.
[35] J.C. Yu, J. Yu, W. Ho, Z. Jiang, L. Zhang, Effects of F—Doping on the photocatalytic activity and microstructures of nanocrystalline TiO_2 powders, Chem. Mater. 14 (2002) 3808–3816.
[36] J. Liqiang, Q. Yichun, W. Baiqi, L. Shudan, J. Baojiang, Y. Libin, F. Wei, F. Honggang, S. Jiazhong, Review of photoluminescence performance of nano-sized semiconductor materials and its relationships with photocatalytic activity, Sol. Energy Mater. Sol. Cells 90 (2006) 1773–1787.
[37] M. Senthilnanthan, D.P. Ho, S. Vigneswaran, H.H. Ngo, H.K. Shon, Visible light responsive ruthenium-doped titanium dioxide for the removal of metsulfuron-methyl herbcide in aqueous phase, Sep. Purf. Technol. 75 (2010) 415–419.
[38] M.M. Niyaz, Photocatalytic ozonation of dyes using copper ferrite nanoparticle prepared by co-precipitation method, Desalination 279 (2011) 332–337.